Water Research 176 (2020) 115748

Contents lists available at ScienceDirect

Water Research

journal homepage: www.elsevier.com/locate/watres

Biofouling, metal sorption and aggregation are related to sinking of microplastics in a stratified reservoir

Rico Leiser [a, *], Gi-Mick Wu [b], Thomas R. Neu [c], Katrin Wendt-Potthoff [a]

[a] Department of Lake Research, Helmholtz Centre for Environmental Research, Brückstraße 3a, 39114, Magdeburg, Germany
[b] Helmholtz Centre for Environmental Research, Permoserstraße 15, 04318, Leipzig, Germany
[c] Department of River Ecology, Helmholtz Centre for Environmental Research, Brückstraße 3a, 39114, Magdeburg, Germany

ARTICLE INFO

Article history:
Received 13 October 2019
Received in revised form
14 March 2020
Accepted 20 March 2020
Available online 25 March 2020

Keywords:
Microplastics
Reservoirs
Biofouling
Aggregation
Microscopy
Sinking

ABSTRACT

Microplastic particles entering aquatic systems are rapidly colonized by microbial biofilms. The presence of microbial biomass may cause sinking of particles and as a consequence prevent their transport to the oceans. We studied microbial colonization of different polymer particles exposed in the epi-, meta- and hypolimnion of a freshwater reservoir during late summer for 47 days. Parameters measured included biofilm formation, metal sorption and sinking velocities. Microbial biofilms contained bacteria, cyanobacteria and algae as well as inorganic particles such as iron oxides. Regardless of biofilm thickness and biovolumes of different biofilm constituents, single polyethylene (PE) particles stayed buoyant, whereas the sinking velocity of single polystyrene (PS) and polyethylene terephthalate (PET) particles did not change significantly compared to initial values. During exposition, a mixing event occurred, by which anoxic, iron-rich water from the hypolimnion was mixed with water from upper layers. This induced aggregation and sinking of hypolimnetic PE particles together with organic matter, cyanobacteria colonies and iron minerals.

© 2020 Elsevier Ltd. All rights reserved.

1. Introduction

Microplastics (MP) are one of the widely distributed man-made pollutants, found in nearly any place of the earth. Zones with reduced flow velocities such as point bars, impoundments and reservoirs allow particles to settle down to the sediment (Watkins et al., 2019), reducing the plastic load of streams (Castañeda et al., 2014). As a consequence, high concentrations of MP are found in sediments of natural lakes (Anderson et al., 2017) and man-made reservoirs (Zhang et al., 2015), which may even act as permanent sink (Corcoran et al., 2015). Elucidating the factors governing particle settling in zones with reduced flow, such as reservoirs, is therefore crucial for a comprehensive understanding of MP transport in the environment.

Microplastic particles are rapidly colonized by various microorganisms like bacteria, cyanobacteria and microalgae when submerged in freshwater. This leads to the development of a biofilm comprising microbial communities distinct from the surrounding water (Zettler et al., 2013). Environmental conditions such as pH, temperature, light/oxygen availability or dissolved nutrients mainly determine which organisms may occur within a biofilm; whereas the surface properties seem to be less influential than these external factors (McCormick et al., 2014; Oberbeckmann et al., 2016). However, if incubated under the same environmental conditions, differences between microbial community composition and biofilm density can be observed among different surfaces (Parrish and Fahrenfeld, 2019).

The settling of particles is influenced by their shape, size and density (Chubarenko et al., 2016; Kowalski et al., 2016). Particles denser than water and above 5 μm in diameter will eventually settle down by gravitational force within a few meters after being submerged in water. Particles less dense than water or below 5 μm in size may stay buoyant or even float at the surface if not altered by environmental processes (Besseling et al., 2017). For further transport, aggregation with natural materials and colonization by organisms play a crucial role by increasing the size and density of these particles. In oceans, the aggregation of buoyant MP with algae (Long et al., 2015) and marine snow (Michels et al., 2018) leads to rapid settling. Coverage of larger particles with calcareous macroorganisms, which is often referred to as biofouling, also sinks buoyant plastic polymers (Kaiser et al., 2017).

* Corresponding author.
E-mail address: rico.leiser@ufz.de (R. Leiser).

https://doi.org/10.1016/j.watres.2020.115748
0043-1354/© 2020 Elsevier Ltd. All rights reserved.

Conditions in freshwater differ from the marine environment with regard to physical (currents/waves, tides, wind, temperature), chemical (pH, salinity, oxygen availability, nutrients/metals) and biological parameters. Additionally, the residence time in freshwater reservoirs is by magnitudes lower than in the ocean, leading to the assumption that extensive aging and biofouling by heavy calcareous organisms is unlikely to take place. Transfer of buoyant MP to reservoir sediments may therefore rely rather on mechanisms distinct from those observed in marine environments (Besseling et al., 2017). During summer, many reservoirs become stratified and partly anoxic, leading to the reduction of iron oxides to ferrous iron. Lake mixing leads to the autoxidation of ferrous iron and formation of iron oxide colloids in the water column (Tipping et al., 1981). These colloids are known to sink together with algae and cyanobacteria by forming sticky agglomerates with the cells (Oliver et al., 1985).

We hypothesize that this aggregation may also be relevant for MP during mixing. Stratified reservoirs, which exhibit gradients of redox potential and oxygen availability, may therefore provide an ideal setting to study the factors governing biofilm development and plastic sedimentation which are presently not well understood. We characterized biofilm formation on PE, PET and PS in the stratified mesotrophic Malter reservoir during late summer. Other factors such as aggregation with freshwater algae and cyanobacteria or sorption of metals were considered as well. The following hypotheses were tested: i) incubation depth and time influence biofilm composition; ii) biofilm covered MP sorb metal oxides; iii) aggregation or biofouling influence MP settling in stratified reservoirs.

2. Materials and methods

2.1. Location

The mesotrophic Malter reservoir (0.84 km^2, 335 m above sea level) is located in eastern Germany (Dippoldiswalde, Saxony). Its maximum depth is 16–20 m and the maximum storage capacity is 9.6 million m^3. Due to continuous discharge during summer, the water level may drop by several meters. In summer the water column is stratified with an anoxic hypolimnion separated from the oxic epilimnion by a thermocline at 8 m depth in 2018 (Fig. S1 and Table S1). Autumnal mixing usually occurs during September restoring oxic conditions near the bottom (Müller et al., 2000).

2.2. Plastic material and incubation conditions

Three different polymer foils in research quality and free of stabilizers, PE (ρ: 0.924 g cm^{-3}, contact angle: 99.2 ± 4.1°, ET311251), PS (ρ: 1.05 g cm^{-3}, contact angle: 91.7 ± 4.6°, ST311125), and PET (ρ: 1.4 g cm^{-3}, contact angle: 84.3 ± 3.4°, ES301425) were purchased from GoodFellow (Hamburg, Germany). Foil thicknesses were 0.125 mm for PS/PET and 0.15 mm for PE. Polymer squares (4 × 4 mm) were obtained employing a multiple puncher (Pavo HD Wire Binder), using sterile techniques (ethanol-sterilized puncher and lab cloths, laminar flow bench). PS particles exhibited a curved shape, whereas PE and PET particles were even. The cutting edges of the particles were rougher compared to the uncut foil. The squares and foils were stored at 20 °C in a dry, dark place.

In order to incubate the particles in Malter reservoir, 500 particles of each polymer (PE, PS, PET) were transferred to individual closed stainless steel cages (cylindrical shape, diameter 10 cm, length 25 cm, mesh width 3 mm) each containing just a single polymer type (Arias-Andres et al., 2018). Particles were distributed to the cages as follows: 3 × 500 particles (three individual cages containing PE, PET or PS) in the epilimnion, 3 × 500 in the metalimnion and 9 × 500 (in 3 × 3 cages with PE, PET or PS) in the hypolimnion (Fig. S2). Cages were incubated from August 30 to October 16, 2018, with three samplings after 6 days (09/05), 22 days (09/21) and 47 days (10/16). Three incubation depths at 0.5 m (epilimnion, O_2 saturation > 100%, light), 8 m (metalimnion, O_2 saturation 80%, no light) and 16 m (hypolimnion, O_2 saturation 0%, no light) were chosen according to prevailing oxygen concentrations (multi-parameter probe, Sea & Sun Technologies, Germany) and light intensities (Licor 1400, Li-cor Biosciences, Germany) on August 30 (Fig. S1a). Cages were lifted to the surface for sampling and particles were gently transferred using tweezers or flushing with reservoir water to pre-combusted (450 °C, 4 h) glass Petri dishes filled with water from the incubation depth. The hypolimnion was anoxic during the initial stage of the experiment (Fig. S1). To avoid repeated oxygen exposure of anaerobic organisms during lifting of the cages for sampling, additional cages on separate ropes were deployed in the hypolimnion so that for each sampling previously un-sampled cages were used. Some PS particles were flushed out of the cages, leading to missing values of crystal violet staining in the epilimnion and metalimnion for day 47. All samples were stored in the dark at 4 °C until processing in the laboratory. Samples for confocal laser scanning microscopy (CLSM) were preserved in 4% formalin solution, and particles for iron/manganese measurement were directly placed in glass vials with hydroxyl ammonium chloride-hydrochloric acid (0.5 M/1 M). Particles used to determine the sinking velocity and for conducting crystal violet staining were transported in reservoir water.

2.3. CLSM imaging

At every sampling date 10 randomly chosen particles per polymer were taken from each incubation depth, and 5 random locations on each of them were examined via CLSM. Samples were washed in tap water and mounted in a 5 cm Petri dish. For this purpose the plastic squares were glued with silicone adhesive to the bottom of the dish. Nucleic acid staining was done with SybrGreen (dilution 1:1000). After staining for 5 min the Petri dish was flooded with tap water. For CLSM a TCS SP5X with upright microscope and super continuum light source was available. The system was controlled by LAS AF version 2.4.1. Samples were examined by using a long working distance 63x NA 0.9 water immersible objective lens. Excitation was at 490, 561 and 633 nm. Emission was recorded sequentially from 480 to 500 nm (reflection), 510–580 nm (SybrGreen) together with 650–720 nm (autofluorescence of chlorophyll *a*) and separately from 575 to 650 nm (autofluorescence of phycobilins). Datasets were recorded without average and a step size of 1 μm. For visualisation Imaris (Bitplane) version 9.3 was employed. Projected image data sets were printed from photoshop (Adobe). Calculations of cell biovolumes contained in the digital images were done with an adapted version of ImageJ (Staudt et al., 2004). Extracellular polymeric substances (EPS) were visualized by the glycoconjugate binding lectin AAL-A568 (Vector Laboratories, Burlingame, USA).

2.4. Iron and manganese analysis

Iron and manganese were determined by extracting 15 pooled particles per sampling date, depth, and polymer type with 2 ml hydroxyl ammonium chloride-hydrochloric acid solution (0.5/1 M) for 24 h in an overhead shaker (120 rpm). Iron was subsequently measured by ferrozine assay (Stookey, 1970) at 562 nm using a spectrophotometer (Agilent Cary 60 UV-VIS). Briefly, 50 μl of acidic, centrifuged sample (10 min, 15000 rpm) was added to 950 μl ferrozine solution (50 mM HEPES, 1 mg ml^{-1} ferrozine, pH 7.0) and incubated for 10 min prior to the measurement. If optical density

exceeded 1.0 the remaining sample was diluted with acidified ultra-pure H_2O prior to the addition of ferrozine. Manganese was measured using the formaldoxime method adapted from Burlage et al. (1998), Goto et al. (1962) and Brewer and Spencer (1971). The following solutions were prepared: (1) TRIS-Buffer (5 M TRIS-HCl, pH 9.0 adjusted with H_2SO_4), (2) formaldoxime (20 g hydroxyl ammonium chloride in 450 ml ultrapure H_2O, addition of 10 ml 10% formaldehyde, filled up to 500 ml), (3) 0.1 M EDTA in water and (4) 10% hydroxyl ammonium chloride in water. One ml of TRIS solution was added to an Eppendorf tube followed by addition of 100 µl supernatant from the centrifuged sample. Then 100 µl of formaldoxime was added, followed by 2 min of incubation at room temperature. To remove dissolved ferrous iron, 100 µl EDTA and 200 µl hydroxyl ammonium chloride solution were added separately, subsequently the solution was incubated at room temperature for 10 min and measured at 450 nm (Agilent Cary 60 UV-VIS).

2.5. Crystal violet staining

Crystal violet staining was conducted to quantify total biofilm mass (Arias-Andres et al., 2018), as the dye stains both cells and the biofilm EPS (Xu et al., 2016). On each sampling date 8 particles from each depth and of every polymer type were stained. During the procedure some particles were lost leading to lower sample numbers (Fig. 2). Briefly, particles were dried (60 °C, 24 h), stained with 250 µl crystal violet (0.3% in ultrapure water) for 15 min, washed 4 times with ultrapure water and de-stained with 200 µl ethanol (97%). The ethanol-crystal violet solution was measured at 595 nm (OD_{595}) using a multiplate reader (Thermo Fisher Multiscan RC). Samples showing optical densities higher than 1.00 were diluted with 97% ethanol.

2.6. Measurement of sinking velocities

Sinking velocities were determined within 12 h after sampling. A sinking column (0.15 m × 2 m) filled with deionized water and placed in a climate chamber (20 °C) was used. The water was filled 2–3 days in advance to avoid currents and temperature differences in the column. The time needed to settle 50 cm through the column was measured using a stop watch (Kaiser et al., 2017). Particles were placed carefully beneath the water surface using tweezers and then allowed to settle for 30 cm in order to reach their terminal velocity before measurement was started. Particles settling close to the tube walls were excluded from data analyses. Multicellular organisms attached to sinking polymers were identified via binocular and a field guide (Streble and Krauter, 1988) to the family level.

2.7. Analysis of iron colloids

Iron colloids resulting from reservoir mixing were obtained by centrifuging two water samples retrieved on September 21 (10 min, 15000 rpm). The resulting pellets were dried (60 °C for 24 h) and iron and manganese were analysed according to methods described in 2.4. The remaining solids were washed three times with acidified water (pH 1.8) and centrifuged/dried again (60 °C, 24 h) to determine the acid soluble fraction. Afterwards the ash content was determined by combusting the sample at 450 °C for 24 h. One aggregate formed by PE and iron colloids was treated similarly and analysed for its iron and manganese content.

2.8. Data analysis

The critical thickness and mass of an attached fouling film in order to overcome a PE squares buoyancy was calculated following Chubarenko et al. (2016):

$$d_{film} = \frac{h}{2} * \frac{\rho_w - \rho_0}{\rho_f - \rho_w} \quad (1)$$

$$m_f = a^2 * d * \rho_f \quad (2)$$

With ρ_0: Density of unfouled PE particle (920 kg m^{-3}); ρ_f: Density of the fouling film (different densities, Table S2); ρ_w Density of water (1000 kg m^{-3}); h : Height of the particle (1.5×10^{-4} m); d_{film}: Thickness of the fouling film; m_f: Mass of fouling film needed to sink PE; a: Length of LDPE particle (4×10^{-3} m).

Results were compared among sampling dates and depths using non-parametric bootstrapping (Efron and Tibshirani, 1986) because assumptions of the ANOVA were not satisfied. For each comparison, we reported the median difference of 10000 bootstrapped samples with 95% confidence intervals. Differences in medians containing values other than zero were regarded as significantly different from each other by 95% chance. Software R (R Core Team, 2018) was used for all statistical analysis.

3. Results

3.1. Biovolumes analysed by CLSM

Biovolumes of three phylogenetic groups (bacteria, cyanobacteria and algae) were analysed for three different reservoir depths (epilimnion, metalimnion and hypolimnion) and time intervals (day 6, day 22 and day 47). Cages from the epilimnion were covered with visible biofilms after 47 days, whereas no visible biofilm formation was observed on cages from the metalimnion and hypolimnion.

The cellular components of the biofilms on day 6 consisted predominantly of bacteria (Fig. 1). PET had fewer bacteria compared to PS/PE in the metalimnion and to PE in the epilimnion, while PS had significantly more bacteria than PE and PET in the hypolimnion. Cyanobacteria and algae were scarce throughout, nonetheless small but statically significant differences among the polymers were found (Fig. 1b and c).

On day 22 (Fig. 1) biofilms were again dominated by bacteria. PE showed the highest bacterial biovolume of all polymers in each incubation depth (Fig. 1a). PS had higher values than PET in the epilimnion and metalimnion, but lower bacterial biovolumes in the hypolimnion compared to PET. Cyanobacteria biovolumes were again negligible. Some algae were found on PS exceeding PE and especially PET in the epi- and metalimnion. In the hypolimnion PE had remarkably higher algae biovolumes than PET and PS.

Biovolumes on day 47 were distinct from the previous sampling dates, and characterized by higher shares of phototrophic organisms in the epilimnion. Bacterial biovolume showed less pronounced differences between the surfaces than before. Cyanobacteria in the epilimnion made up a significant proportion of the phototrophic biovolume. Comparing the surfaces, PET and PS showed the highest volumes, while PE only reached around 5% of the cyanobacteria biovolume found on PET or PS. In the metalimnion cyanobacteria were scarce throughout. In the hypolimnion cyanobacteria biovolume was low but significantly different between surfaces (Fig. 1c). Substantial algae biovolumes were found on all polymers in the epilimnion with PET/PS significantly exceeding PE. Few algae occurred in the metalimnion and hypolimnion although some significant differences were found (Fig. 1b).

The biovolumes of bacteria, cyanobacteria and algae increased over time on all polymers in each of the incubation depths. Remarkably, algal biovolumes increased by at least one order of magnitude between day 22 and day 47 in the epilimnion. No

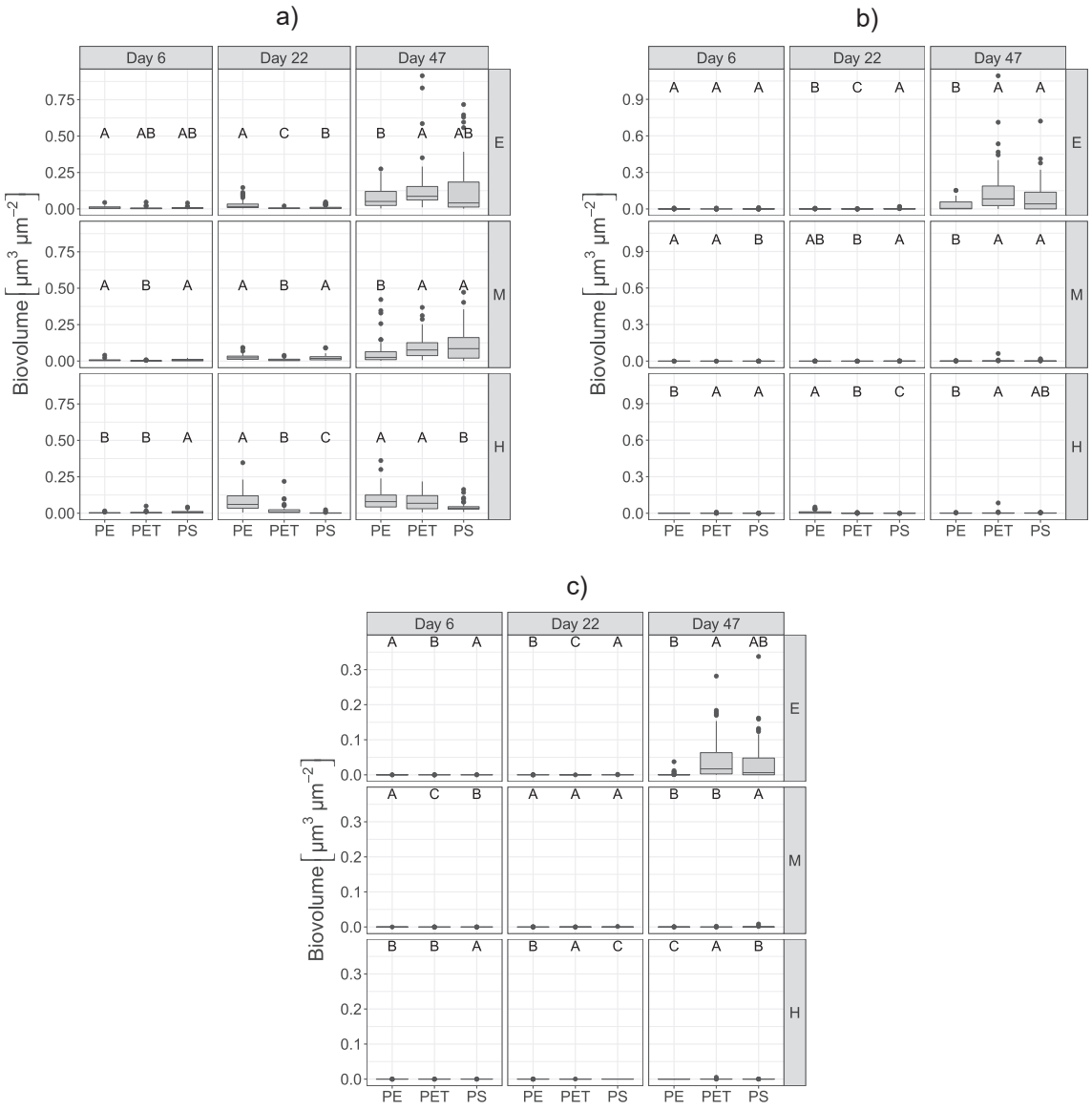

Fig. 1. Biovolumes of bacteria (a), algae (b) and cyanobacteria (c) in epilimnion (E), metalimnion (M) and hypolimnion (H) over 47 days of exposure. Sample sizes were 50 for each polymer. Groups significantly different from each other (with 95% confidence) are highlighted with letters in alphabetical order beginning with the highest value in each individual panel.

general differences regarding the final bacterial biovolumes were found at day 47. However, PE tended to have lower biovolumes of phototrophic organisms than the other surfaces.

3.2. Biofilms analysed by crystal violet staining

On day 6 the biofilm was not well established, with OD_{595} values being low for all polymers (Fig. 2), but still significantly higher than the pristine particles used as blanks. Differences between the polymers were scarce with only PET exhibiting lower OD_{595} values than PE in all samples on day 22 and day 47. Biofilm mass on PS on day 22 was equal to that on PE in the epilimnion and metalimnion but lower than on PE in the hypolimnion. PS values were equal to PET values on day 22 except for the epilimnion. OD_{595} was highest at day 47 for all sampled polymers, which indicates an increase of stainable molecules over the incubation time.

The OD_{595} values showed a positive linear correlation with their respective total biovolumes (sum of algae, bacteria and cyanobacteria) derived from CLSM imaging. The increase of OD_{595} per biovolume was higher for PE than for PET, as expressed by a steeper regression line. Therefore higher OD_{595} values would result from similar or lower biovolume on PE compared to PET (Fig. S3, Table S3).

3.3. Metal concentrations on MP

Iron and manganese (detection limit 0.3 µg mg^{-1}) were found on all tested biofilm-covered MP. On day 6 and 22 no manganese was detected, but after 47 days manganese was found on every polymer in most incubation depths. PE showed the highest manganese sorption, exceeding 0.63 µg mg^{-1} in the epilimnion.

In contrast, iron was detected from day 6 on at all polymers. On day 22 substantial iron sorption was observed in the hypolimnion (Fig. 3). The highest iron concentration occurred on PE on day 47 in the epilimnion (1.64 µg mg^{-1}).

At least for PE metal concentrations increased substantially over

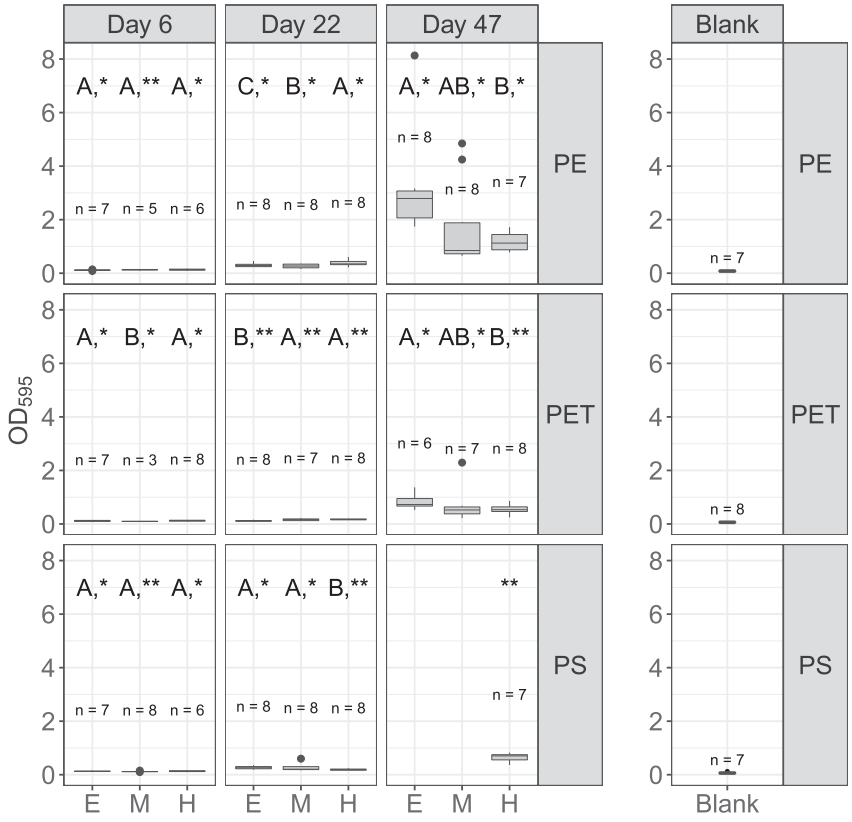

Fig. 2. Effect of incubation depth and exposure time on the total biofilm mass (crystal violet staining, OD_{595}). Pristine particles were used as blanks. Values for PS are missing on day 47 for the epilimnion and metalimnion due to sample loss. Letter display significant differences (with 95%confidence) between the surface in each panel in horizontal direction, stars (with * > **) mark significant difference between the incubation depths of a single polymer in vertical direction.

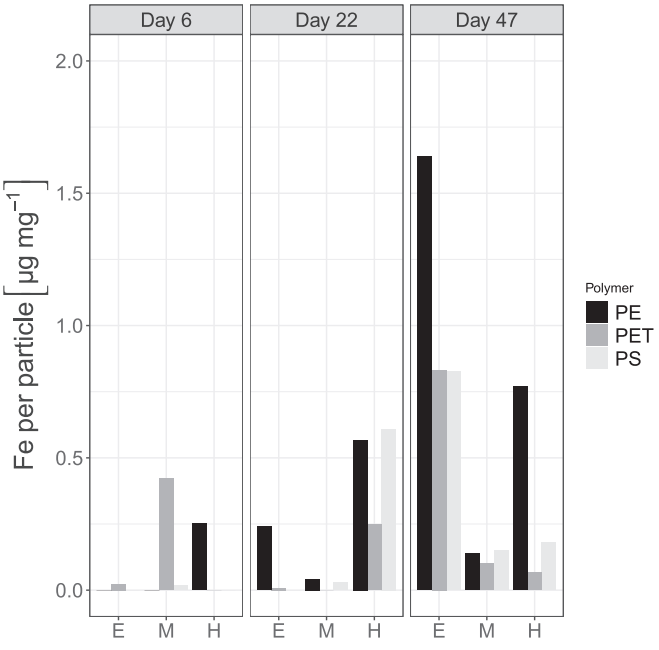

Fig. 3. Iron concentrations on plastic polymers during exposure in Malter reservoir. Missing values indicate no measurable iron present at the particular time point or depth. The values were calculated by dividing the measured concentrations by particle weight (15 particles weighing 1.93 (PS), 2.63 (PET) and 2.2 mg (PE) each).

the incubation time. Sorption of iron exceeded that of manganese on all polymers. As the data display an integrated mean of 15 particles per measurement no statistical analysis was conducted.

3.4. Sinking velocity of particles

During the experiment no sinking of single PE particles regardless of incubation depth or time occurred and so no sinking velocities were recorded.

The terminal sinking velocities of PET squares were roughly three times higher than those of PS, with values of 0.028 m s^{-1} compared to 0.0075 m s^{-1} respectively (Fig. 4). No substantial differences between incubated particles and the control pristine particles of PET and PS were observed (Table S4). Small differences between some incubation depths or sampling dates were occurring (Table S4). On day 47, larger organisms such as hydras and cladocerans were attached to the surface of 9% of the PS particles and 10% of the PET particles used in the sinking experiment. These organisms influenced the sinking speed of PS slightly by accelerating the sinking speed by 4% (median of particles with attached multicellular organisms: 0.008 m/s, n: 4) and decreased the sinking speed of PET by 1% (median: 0.0276, n: 6) compared to particles with no attached larger organisms. On day 6 and day 22 no such organisms were observed on the particles.

3.5. Mixing event and aggregation of MP with iron colloids

Oxygen intruded into the anoxic hypolimnion of the stratified Malter reservoir between September 5 (day 6) and September 21 (day 22) (Fig. S1b and c). Substantial amounts of brownish-red iron

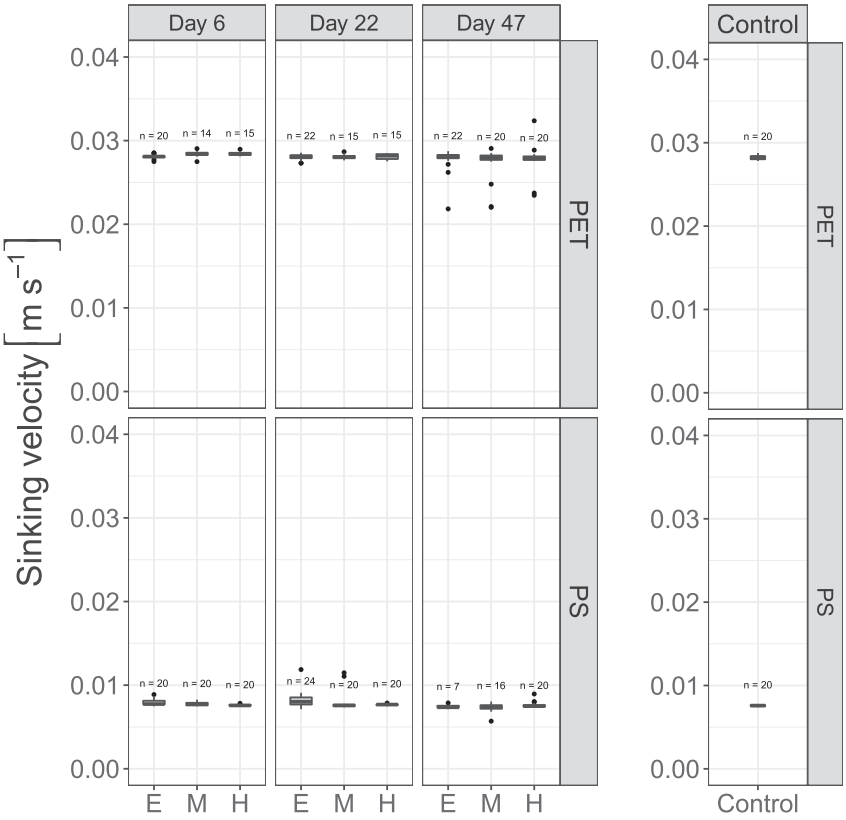

Fig. 4. Sinking velocity of PET and PS in deionized water (20 °C) after incubation in Malter reservoir. The control displays settling velocities of unexposed (pristine) particles.

flocs (Fig. 5a) floated freely in the whole water column on September 21. These reservoir-borne iron colloids consisted of approximately 12% per weight iron, 40% per weight organics, and 38% per weight ash content referring to the dry mass. The acid soluble fraction was 26% per weight which corresponds well to the mass of 27% Fe_2O_3 x 0.5 H_2O stoichiometrically calculated from the measured iron content. The colloids were not observed at day 47 (October 16). Aggregation of four PE particles with iron colloids was observed in the hypolimnion (Fig. 5a and b). The formed aggregate was stable enough for being transferred by tweezers without breaking apart. Its density was higher than water; subsequently it sank down to the bottom of a water filled storage container. Non-agglomerated PE particles retrieved from the hypolimnion on that day remained buoyant. The biofilm on the aggregate showed higher biovolumes of bacteria, algae and cyanobacteria compared to any other surface (Fig. 5c). The agglomerate was of brownish color, indicating the presence of iron which made up approximately 3% Fe (11 μg mg^{-1}) of the total dry mass. Small amounts of manganese reaching <1% (0.07 μg mg^{-1}) of the total dry mass were measured as well.

4. Discussion

In this study we measured biofilm formation and sorption of metals to different polymers in MP size in order to investigate the effects on their sinking behavior. Employing CLSM, crystal violet staining and spectrophotometric methods, we found microbial biofilm formation to be not sufficient for promoting the sinking of single MP particles in Malter reservoir during late summer. Sinking through aggregation with iron colloids and biomass (cells/EPS) was observed after reservoir mixing in a single case.

Contrary to our findings, biofouling with cyanobacteria was found to sink polypropylene particles in a eutrophic tropical lake (Chen et al., 2019). The authors hypothesized that the binding of inorganic material contributed more significantly to the mass of the fouling film than the phototrophic cells (Chen et al., 2019). Differences to our results can be explained by distinct environmental conditions in Malter reservoir such as lower concentrations of chlorophyll *a* (41 μg/l vs. 120 μg l^{-1}), phosphate (0.03 vs. 0.214 mg l^{-1}), ammonia (0.07 vs. 0.41 mg l^{-1}), and suspended solids (4 vs. 35 mg l^{-1}). Regarding the different conditions, biofouling will be more intense in warm, nutrient-rich, shallow lakes compared to temperate, nutrient-poor, deep reservoirs. The absence of calcareous macrofoulers which is considered as a major factor promoting sinking of MP in marine environments (Kaiser et al., 2017) may also explain low impact of biofouling on the particle densities in this study.

However it cannot be excluded that more extensive biofouling occurs during different seasons and may facilitate MP sinking in Malter reservoir. Biofilm formation may strongly influence aggregation dynamics and subsequently the sinking of MP by increasing the stickiness, surface charge or altering the morphology (e.g. lobes, filaments) of the particles. Aggregation with inorganic and organic particles is considered as another important process that determines the environmental fate of MP (Besseling et al., 2017). Sticky organic material such as marine snow (Porter et al., 2018), biogenic particles (Michels et al., 2018), EPS (Summers et al., 2018), organo-mineral particulate matter (Möhlenkamp et al., 2018) and marine (Long et al., 2015) or freshwater microalgae (Lagarde et al., 2016) can sink buoyant MP through formation of large hetero-aggregates. Most studies used laboratory set-ups employing conditions favoring aggregation such as low shear stress and high particle concentrations (10^1-10^4 particles ml^{-1}) (Möhlenkamp et al., 2018) which may not reflect natural conditions. Currents,

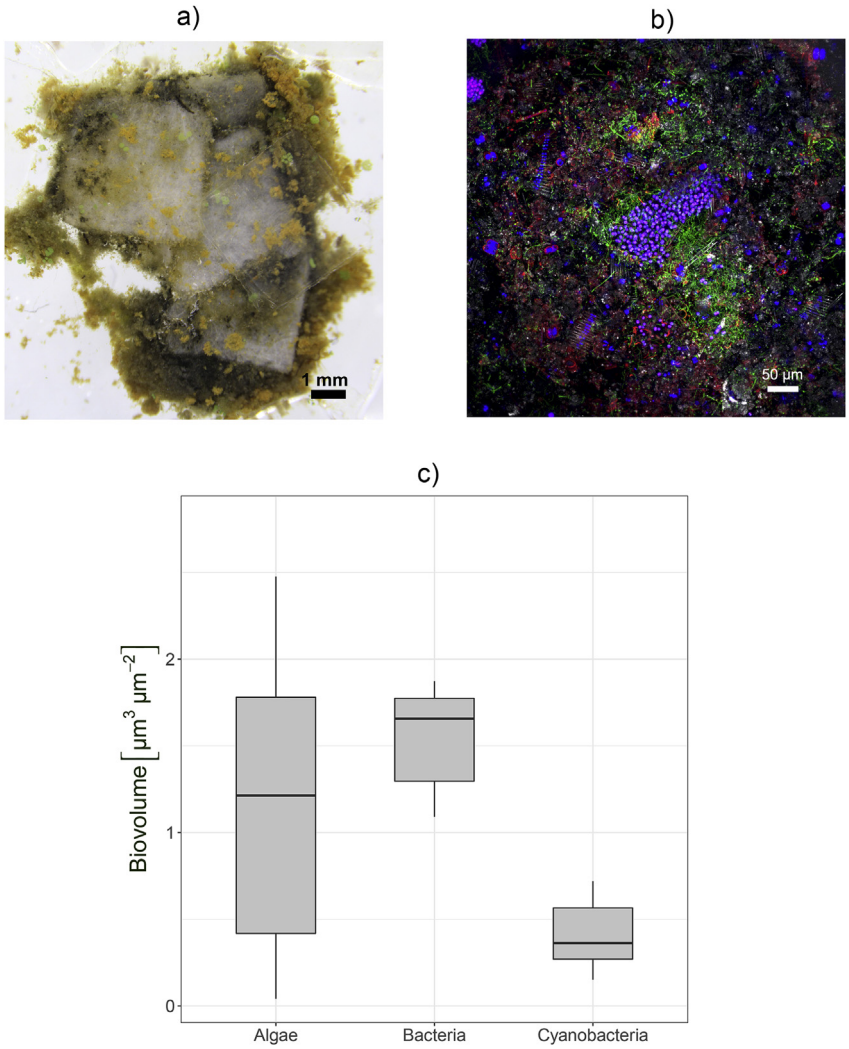

Fig. 5. Images and biovolumes of PE aggregate from hypolimnion at day 22. a) bright light microscopy (10x magnification), b) CLSM image stained with lectin to visualize EPS, c) biovolumes of algae, bacteria and cyanobacteria within the aggregate. Coding for CLSM: green (bacterial cells), purple (cyanobacteria), blue (algae), and red (EPS). (For interpretation of the references to color in this figure legend, the reader is referred to the Web version of this article.)

grazing, microbial degradation and ingestion by larger organisms could lead to rapid break-up or consumption of such aggregates in nature (Cole et al., 2016). In this study aggregation of PE with organo-mineral matter was observed. The formation right after mixing indicates that iron oxide containing colloids induced the aggregation of PE with organic matter and cells of cyanobacteria, algae and bacteria. Iron colloid formation is an important process capable to aggregate and sink buoyant cyanobacteria in natural lakes after mixing (Oliver et al., 1985). Given that only 4 large microplastic particles aggregated with such colloids; this study cannot provide sufficient data on the importance and implications of this mechanisms for the fate of MP in reservoirs. Furthermore it should be considered that reservoir mixing is no prerequisite for the aggregation and subsequent settling of MP in the environment.

Considering the oxic conditions of the hypolimnion prevailing at least since day 22, the majority of iron and manganese should have been present as metal oxides. Oxide minerals such as ferrihydrite (Fe_5HO_8 x 4 H_2O), magnetite (Fe_3O_4) or manganese (IV) oxide (MnO_2) exhibit a high specific density and may influence the density of MP particles. The density change of PE particles (4 × 4 × 0.15 mm) covered by a "fouling film" was calculated by using the specific density of these minerals as input variable (Chubarenko et al., 2016). Afterwards the mass of fouling films comprising ferrihydrite, magnetite, manganese oxide or bacteria needed to sink the PE particle ($\rho_{PE} > \rho_{Water}$) were determined following equation (2). Accordingly, the mass concentrations needed to sink PE are 54 µg mg^{-1} magnetite, 58 µg mg^{-1} ferrihydrite, 55 µg mg^{-1} manganese oxide and 131, 156 or 218 µg mg^{-1} bacteria (with different $\rho_{Bacteria}$, Table S2). The maximum iron concentration found on buoyant PE (1.64 µg mg^{-1}) corresponded to 2.2 µg mg^{-1} ferrihydrite or 2.1 µg mg^{-1} magnetite whereas the maximum manganese concentration (0.64 µg mg^{-1}) corresponded to 0.94 µg mg^{-1} manganese oxide. Therefore, the mass concentration of metals bound to freely floating PE particles was at least one order of magnitude too low to overcome their buoyancy. The sinking aggregated PE particles showed iron concentrations of 11 µg mg^{-1} corresponding to 16.4 µg mg^{-1} ferrihydrite or 15.2 µg mg^{-1} magnetite. Biovolume (in µm^3 µm^{-2}) of bacteria, cyanobacteria and algae can be converted to cells mass per particle by multiplying with the particle surface area (1.6 × 10^7 µm^2) and the specific density of microbial biomass (Table S2). Buoyant PE particles contained approximately 8 µg mg^{-1} total biomass (for $\rho_{Biomass}$: 1500 kg m^{-3}) while the microbial biomass on the sunken PE agglomerate made up 149, 138 or 124 µg mg^{-1} depending on the

specific density of microbial biomass applied. The biomass calculated for the sunken agglomerated PE was in good agreement with the 131 μg mg^{-1} (for $\rho_{Biomass}$: 1500 kg m^{-3}) (Chubarenko et al., 2018) theoretically needed to sink buoyant PE particles. Assuming lower $\rho_{Bacteria}$ the results deviated slightly (156 μg mg^{-1} for $\rho_{Biomass}$: 1388 kg m^{-3}) (Besseling et al., 2017) or moderately (218 μg mg^{-1} for $\rho_{Biomass}$: 1250 kg m^{-3}) (Kooi et al., 2017) from the biomass theoretically required for sinking. However it should be considered that most of the aggregate organic mass was not quantified via CLSM as EPS was not assessed with the used technique. Nonetheless ballasting effects of microorganisms considerably exceeded the effect of metal oxides, comprising a likely reason for the observed loss in buoyancy. This leads to the assumption that the aggregation of freshwater microorganisms can sink MP if sufficient biomass is provided. However, under low bio-productivity or low temperature conditions the critical mass to sink the MP may not be reached within reasonable timescales.

The extent of EPS production within the biofilms seemed to differ between the polymers, as shown via crystal violet assay. Algae and cyanobacteria cells were present in lower densities on PE compared to PET and PS as seen from CLSM imaging. This may indicate that these organisms had to put more effort into attachment to PE surfaces than to PET/PS. Low attachment efficiency leads to environmental stress (Vosshage et al., 2018) and ultimately to more EPS production by the stressed cells (Scott et al., 2014). Therefore the fewer but stressed cells on PE could have produced more EPS than the cells on PET.

Regarding the occurrence of metals on biofilm covered MP, PE showed higher concentrations of iron and manganese compared to the other polymers. Concentrations of Fe and Mn exceeded up to 100 times (Fe) or 10 times (Mn) the concentrations found on beached plastic pellets at British shores (Ashton et al., 2010; Holmes et al., 2012) and plastics exposed to seawater for several months (Rochman et al., 2014). Lower ionic strength and the higher abundance of Fe/Mn in freshwater water may explain the higher MP metal concentrations found in this study. According to previous studies long-term metal sorption to plastics does not differ between polymer types (Rochman et al., 2014). The metal sorption is rather controlled by the biofilm thickness and the available binding places therein (Rochman et al., 2014; van Hullebusch et al., 2003). In our study, PE showed the highest crystal violet stainable biomass of all polymers. PE may therefore have provided more binding places for metals within the EPS matrix, leading to the highest measured iron and manganese concentrations.

The polymers were enclosed in steel cages during the experiment. For PS and PET this produces artificial conditions, as particles of the used size will settle down to the sediment within 10 (PET) to 30 min (PS) assuming a mean water depth of 16 m and no other currents or mixing. However, polymers with mechanically changed properties such as PET bottles with trapped air inside or expanded PS may stay afloat for a longer time-span than the particles used in this experiment. This makes the description of biofilm formation on PS and PET in the upper reservoir parts environmentally relevant even though the particles are not buoyant. Conditions for biofilm formation may differ between the interior of the cages and the open reservoir water, as larger grazing organisms were excluded by the mesh size. Furthermore the cages had a shading effect reducing the light intensity by 33%. Due to biofilm formation on the cages this shading effect could have been even stronger than the 33% measured for blank cages. Reservoirs and especially their hypolimnia experience very low currents. For this reason, biofilms are only loosely bound to their carriers, making biofilm loss due to shear stress likely. This may partly explain the high variability of biovolumes on particles of the same material and exposure time. Formation of hetero-aggregates between PE and organo-mineral matter was only observed in the hypolimnion. Therefore, the possible sinking of PE floating at the water surface could not be proven directly. Only one aggregate with four PE particles has been observed hence coincidence cannot be excluded. The experiment was conducted from late summer to autumn which includes lowering of temperatures and light intensities during this time. As the extent of biofouling depends on season (Chen et al., 2019), it cannot be excluded that biofouling-induced sinking may occur during other times of the year.

5. Conclusions

- Late summer biofilm development within a temperate mesotrophic reservoir was not sufficient to facilitate sinking of buoyant MP or increasing the settling velocity of dense MP
- Biofilms grown on PET and PS microplastics in the mesotrophic reservoir contained more phototrophic microorganisms than those on PE microplastics
- Manganese and iron sorbed to biofilm covered microplastics in substantial amounts

Declaration of competing interest

The authors declare that they have no known competing financial interests or personal relationships that could have appeared to influence the work reported in this paper.

Acknowledgements

We thank Ute Kuhlicke for extensive microscopy work and excellent advice, and Corinna Völkner, Martin Wieprecht, Franziska Reggelin and Jana Reichenbach for eminent help with field and laboratory work. Therese Kettner is acknowledged for providing the steel cages. We also thank the Landestalsperrenverwaltung des Freistaates Sachsen (LTV; especially Alice Rau) for providing access to the reservoir and water quality data. The critical comments of anonymous reviewers helped to improve the manuscript. This research was supported by the BMBF project MikroPlaTaS (02WPL1448A).

Appendix A. Supplementary data

Supplementary data to this article can be found online at https://doi.org/10.1016/j.watres.2020.115748.

References

Anderson, P.J., Warrack, S., Langen, V., Challis, J.K., Hanson, M.L., Rennie, M.D., 2017. Microplastic contamination in Lake Winnipeg, Canada. Environ. Pollut. 225, 223–231. https://doi.org/10.1016/j.envpol.2017.02.072.

Arias-Andres, M., Kettner, M.T., Miki, T., Grossart, H.-P., 2018. Microplastics: new substrates for heterotrophic activity contribute to altering organic matter cycles in aquatic ecosystems. Sci. Total Environ. 635, 1152–1159. https://doi.org/10.1016/j.scitotenv.2018.04.199.

Ashton, K., Holmes, L., Turner, A., 2010. Association of metals with plastic production pellets in the marine environment. Mar. Pollut. Bull. 60, 2050–2055. https://doi.org/10.1016/j.marpolbul.2010.07.014.

Besseling, E., Quik, J.T.K., Sun, M., Koelmans, A.A., 2017. Fate of nano- and microplastic in freshwater systems: a modeling study. Environ. Pollut. 220, 540–548. https://doi.org/10.1016/j.envpol.2016.10.001.

Brewer, P.G., Spencer, D.W., 1971. Colorimetric determination of manganese in anoxic waters. Limnol. Oceanogr. 16, 107–110. https://doi.org/10.4319/lo.1971.16.1.0107.

Burlage, R., Atlas, R., Stahl, D., 1998. Techniques in Microbial Ecology, first ed. Oxford University Press. https://doi.org/10.1016/s0580-9517(08)x7011-4.

Castañeda, R.A., Avlijas, S., Anouk Simard, M., Ricciardi, A., 2014. Microplastic pollution in St. Lawrence River sediments. Can. J. Fish. Aquat. Sci. 71, 1767–1771. https://doi.org/10.1139/cjfas-2014-0281.

Chen, X., Xiong, X., Jiang, X., Shi, H., Wu, C., 2019. Sinking of floating plastic debris caused by biofilm development in a freshwater lake. Chemosphere 222,

856–864. https://doi.org/10.1016/j.chemosphere.2019.02.015.
Chubarenko, I., Bagaev, A., Zobkov, M., Esiukova, E., 2016. On some physical and dynamical properties of microplastic particles in marine environment. Mar. Pollut. Bull. 108, 105–112.
Chubarenko, I., Esiukova, E., Bagaev, A., Isachenko, I., Demchenko, N., Zobkov, M., Efimova, I., Bagaeva, M., Khatmullina, L., 2018. Behavior of Microplastics in Coastal Zones, Microplastic Contamination in Aquatic Environments. https://doi.org/10.1016/B978-0-12-813747-5.00006-0.
Cole, M., Lindeque, P.K., Fileman, E., Clark, J., Lewis, C., Halsband, C., Galloway, T.S., 2016. Microplastics alter the properties and sinking rates of zooplankton faecal pellets. Environ. Sci. Technol. 50, 3239–3246. https://doi.org/10.1021/acs.est.5b05905.
Corcoran, P.L., Norris, T., Ceccanese, T., Walzak, M.J., Helm, P.A., Marvin, C.H., 2015. Hidden plastics of Lake Ontario, Canada and their potential preservation in the sediment record. Environ. Pollut. 204, 17–25. https://doi.org/10.1016/j.envpol.2015.04.0093.
Efron, B., Tibshirani, R., 1986. Bootstrap methods for standard errors, confidence intervals, and other measures of statistical accuracy. Stat. Sci. 1, 54–75. https://doi.org/10.1214/ss/1177013815.
Goto, K., Komatsu, T., Furukawa, T., 1962. Rapid colorimetric determination of manganese in waters containing iron. Anal. Chim. Acta 27, 331–334. https://doi.org/10.1016/S0003-2670(00)88510-4.
Holmes, L.A., Turner, A., Thompson, R.C., 2012. Adsorption of trace metals to plastic resin pellets in the marine environment. Environ. Pollut. 160, 42–48. https://doi.org/10.1016/j.envpol.2011.08.052.
Kaiser, D., Kowalski, N., Waniek, J.J., 2017. Effects of biofouling on the sinking behavior of microplastics. Environ. Res. Lett. 12 https://doi.org/10.1088/1748-9326/aa8e8b.
Kooi, M., Van Nes, E.H., Scheffer, M., Koelmans, A.A., 2017. Ups and downs in the ocean: effects of biofouling on vertical transport of microplastics. Environ. Sci. Technol. 51, 7963–7971. https://doi.org/10.1021/acs.est.6b04702.
Kowalski, N., Reichardt, A.M., Waniek, J.J., 2016. Sinking rates of microplastics and potential implications of their alteration by physical, biological, and chemical factors. Mar. Pollut. Bull. 109, 310–319. https://doi.org/10.1016/j.marpolbul.2016.05.064.
Lagarde, F., Olivier, O., Zanella, M., Daniel, P., Hiard, S., Caruso, A., 2016. Microplastic interactions with freshwater microalgae: hetero-aggregation and changes in plastic density appear strongly dependent on polymer type. Environ. Pollut. 215, 331–339. https://doi.org/10.1016/j.envpol.2016.05.006.
Long, M., Moriceau, B., Gallinari, M., Lambert, C., Huvet, A., Raffray, J., Soudant, P., 2015. Interactions between microplastics and phytoplankton aggregates: impact on their respective fates. Mar. Chem. 175, 39–46. https://doi.org/10.1016/j.marchem.2015.04.003.
McCormick, A., Hoellein, T.J., Mason, S.A., Schluep, J., Kelly, J.J., 2014. Microplastic is an abundant and distinct microbial habitat in an urban river. Environ. Sci. Technol. 48, 11863–11871. https://doi.org/10.1021/es503610r.
Michels, J., Stippkugel, A., Lenz, M., Wirtz, K., Engel, A., 2018. Rapid aggregation of biofilm-covered microplastics with marine biogenic particles. Proc. Biol. Sci. 285, 20181203 https://doi.org/10.1098/rspb.2018.1203.
Möhlenkamp, P., Purser, A., Thomsen, L., 2018. Plastic microbeads from cosmetic products: an experimental study of their hydrodynamic behaviour, vertical transport and resuspension in phytoplankton and sediment aggregates. Elementa 6. https://doi.org/10.1525/elementa.317.
Müller, J., Ruppert, H., Muramatsu, Y., Schneider, J., 2000. Reservoir sediments - a witness of mining and industrial development (Malter Reservoir, eastern Erzgebirge, Germany). Environ. Geol. 39, 1341–1351. https://doi.org/10.1007/s002540000117.
Oberbeckmann, S., Osborn, A.M., Duhaime, M., 2016. Microbes on a bottle: substrate, season and geography influence community composition of microbes colonizing marine plastic debris. PLoS One 11, 1–24. https://doi.org/10.1371/journal.pone.0159289.
Oliver, R.L., Thomas, R., Reynold, C.S., Walsby, A.E., 1985. The sedimentation of buoyant *Microcystis* colonies caused by precipitation with an iron- containing colloid. Proc. R. Soc. B 223, 511–528. https://doi.org/10.1098/rspb.1985.0016.
Parrish, K., Fahrenfeld, N.L., 2019. Microplastic biofilm in fresh- and wastewater as a function of microparticle type and size class. Environ. Sci. Water Res. Technol. 5, 495–505. https://doi.org/10.1039/c8ew00712h.
Porter, A., Lyons, B.P., Galloway, T.S., Lewis, C., 2018. Role of marine snows in microplastic fate and bioavailability. Environ. Sci. Technol. 52, 7111–7119. https://doi.org/10.1021/acs.est.8b01000.
R Core Team, 2018. R: A Language and Environment for Statistical Computing.
Rochman, C.M., Hentschel, B.T., Teh, S.J., 2014. Long-term sorption of metals is similar among plastic types: implications for plastic debris in aquatic environments. PLoS One 9. https://doi.org/10.1371/journal.pone.0085433.
Scott, C.E., Jackson, D.A., Zimmerman, A.P., 2014. Environmental and algal community influences on benthic algal extracellular material in Lake Opeongo, Ontario. Freshw. Sci. 33, 568–576. https://doi.org/10.1086/675811.
Staudt, C., Horn, H., Hempel, D.C., Neu, T.R., 2004. Volumetric measurements of bacterial cells and EPS glycoconjugates in biofilms. Biotechnol. Bioeng. 88, 585–592doi. https://doi.org/10.1002/bit.20241.
Stookey, L.L., 1970. Ferrozine - a new spectrophotometric reagent for iron. Anal. Chem. 42, 779–781. https://doi.org/10.1021/ac60289a016.
Streble, H., Krauter, D., 1988. Das Leben im Wassertropfen. Mikroflora und Mikrofauna des Süßwassers, eighth ed. Kosmos Stuttgart.
Summers, S., Henry, T., Gutierrez, T., 2018. Agglomeration of nano- and microplastic particles in seawater by autochthonous and de novo-produced sources of exopolymeric substances. Mar. Pollut. Bull. 130, 258–267. https://doi.org/10.1016/j.marpolbul.2018.03.039.
Tipping, E., Woof, C., Cooke, D., 1981. Iron oxide from a seasonally anoxic lake. Geochem. Cosmochim. Acta 45, 1411–1419. https://doi.org/10.1016/0016-7037(81)90275-1.
van Hullebusch, E.D., Zandvoort, M.H., Lens, P.N.L., 2003. Metal immobilisation by biofilms: mechanisms and analytical tools. Rev. Environ. Sci. Biotechnol. 2, 9–33. https://doi.org/10.1023/B:RESB.0000022995.48330.55.
Vosshage, A.T.L., Neu, T.R., Gabel, F., 2018. Plastic alters biofilm quality as food resource of the freshwater gastropod *Radix balthica*. Environ. Sci. Technol. 52, 11387–11393. https://doi.org/10.1021/acs.est.8b02470.
Watkins, L., McGrattan, S., Sullivan, P.J., Walter, M.T., 2019. The effect of dams on river transport of microplastic pollution. Sci. Total Environ. 664, 834–840. https://doi.org/10.1016/j.scitotenv.2019.02.028.
Xu, Z., Liang, Y., Lin, S., Chen, D., Li, B., Li, L., Deng, Y., 2016. Crystal violet and XTT assays on *Staphylococcus aureus* biofilm quantification. Curr. Microbiol. 73 (4), 474–482. https://doi.org/10.1007/s00284-016-1081-1.
Zettler, E.R., Mincer, T.J., Amaral-Zettler, L.A., 2013. Life in the “plastisphere”: microbial communities on plastic marine debris. Environ. Sci. Technol. 47, 7137–7146. https://doi.org/10.1021/es401288x.
Zhang, K., Gong, W., Lv, J., Xiong, X., Wu, C., 2015. Accumulation of floating microplastics behind the Three Gorges Dam. Environ. Pollut. 204, 117–123. https://doi.org/10.1016/j.envpol.2015.04.023.